NASA
Technical Memorandum 107439

Army Research Laboratory
Technical Report ARL–TR–1354

Thermal Fatigue Testing of ZrO_2-Y_2O_3 Thermal Barrier Coating Systems Using a High Power CO_2 Laser

Dongming Zhu and Robert A. Miller
Lewis Research Center
Cleveland, Ohio

Prepared for the
International Conference on Metallurgical Coatings and Thin Films
sponsored by the Vacuum Metallurgy Division and Thin Film Division
of the American Vacuum Society
San Diego, California, April 21–25, 1997

National Aeronautics and
Space Administration

U.S. ARMY
RESEARCH LABORATORY

THERMAL FATIGUE TESTING OF ZrO_2-Y_2O_3 THERMAL BARRIER COATING SYSTEMS USING A HIGH POWER CO_2 LASER

Dongming Zhu † and Robert A. Miller
National Aeronautics and Space Administration
Lewis Research Center, Cleveland, OH 44135

ABSTRACT

In the present study, the mechanisms of fatigue crack initiation and propagation, and of coating failure, under thermal loads that simulate diesel engine conditions, are investigated. The surface cracks initiate early and grow continuously under thermal low cycle fatigue (LCF) and high cycle fatigue (HCF) stresses. It is found that, in the absence of interfacial oxidation, the failure associated with LCF is closely related to coating sintering and creep at high temperatures. Significant LCF and HCF interactions have been observed in the thermal fatigue tests. The fatigue crack growth rate in the ceramic coating strongly depends on the characteristic HCF cycle number, N^*_{HCF}, which is defined as the number of HCF cycles per LCF cycle. The crack growth rate is increased from 0.36 μm/LCF cycle for a pure LCF test to 2.8 μm/LCF cycle for a combined LCF and HCF test at N^*_{HCF} about 20,000. A surface wedging model has been proposed to account for the HCF crack growth in the coating systems. This mechanism predicts that HCF damage effect increases with increasing surface temperature swing, the thermal expansion coefficient and the elastic modulus of the ceramic coating, as well as with the HCF interacting depth. A good agreement has been found between the analysis and experimental evidence.

Keywords: Thermal Barrier Coatings, Thermal High Cycle and Low Cycle Fatigue, Ceramic Sintering and Creep, Characteristic HCF cycle number

INTRODUCTION

The next generation of diesel engines will operate at significantly higher temperatures than current engines. The future low heat rejection engines are designed with improved in-cylinder insulation, increased cylinder pressure and reduced cooling requirements. Heat energy recovery in the exhaust gas by turbocharging and turbocompounding will be incorporated; higher engine fuel efficiency, performance, and reliability can thus be achieved. However, the low heat rejection engine concept inevitably imposes more stringent requirements for engine materials development. Zirconia-based thermal barrier coatings, in particular, have received increasing attention for diesel engine applications. These coatings have low thermal conductivity, relatively high thermal

† National Research Council- NASA Research Associate at Lewis Research Center.

expansivity and excellent mechanical properties. Thereby they can provide thermal insulation to engine components and offer thermal fatigue resistance. The technological challenge is to develop strategies for designing the coatings and the components as a system, with improved reliability and durability in an engine environment. Accomplishing this ultimate goal, however, requires a thorough understanding of the coating attributes and characteristics under the severe temperature and stress cycling conditions encountered in an engine.

Severe thermal transients exist in a diesel engine [1-3]. The start/stop and no-load/full-load engine cycle generates thermal low cycle fatigue (LCF) in the coating system; in addition, the in-cylinder combustion process generates thermal high cycle fatigue (HCF), with a typical frequency on the order of 10 Hz. The HCF transient can generate a temperature fluctuation of more than 200°C that will be superimposed onto the steady-state engine temperature at the coating surface [1, 2, 4]. Under these temperature transients, the failure mechanisms of thick thermal barrier coatings are expected to be very complex. The coating failure is related not only to thermal expansion mismatch and oxidation of the bond coats and substrates [5-7], but also to the steep thermal stress gradients induced from the temperature distributions during the thermal transients in the coating systems [2, 5, 7-10] . The thermal HCF component, when interacts with thermal LCF component, has detrimental effect on coating fatigue life [11] .

The ceramic coating failure under severe thermal cycling conditions is closely related to surface cracking and associated multiple delaminations [7]. Although it has been reported [8, 12] that stresses generated by a thermal transient can initiate surface and interface cracks in a coating system, the mechanisms of the crack propagation and of coating failure under the complex LCF and HCF conditions are not well understood. The interaction between LCF and HCF cycles, and the influence of relative magnitudes of the LCF and HCF transients on coating fatigue life, are among the most important aspects in understanding the thermal fatigue behavior of the coating systems. In this paper, thermal fatigue behavior of an yttria partially-stabilized zirconia coating system is investigated under simulated LCF and HCF engine conditions. The effect of LCF and HCF parameters on fatigue crack initiation in the coating is described. The crack propagation kinetics under LCF and HCF conditions are compared from experimental results to elucidate the detailed coating fatigue mechanisms.

EXPERIMENTAL MATERIALS AND METHODS

Materials and Specimen Preparation

ZrO_2-8 wt % Y_2O_3 ceramic coating and Fe-25Cr-5Al-0.5Y bond coat were plasma-sprayed onto 4140 and 1020 steel substrates using commercially available plasma spray systems and a 6-axis industrial robot. The plasma spray conditions used for both the ceramic coating and

bond coat have been given previously [11] . The substrate configurations used were 4140 steel rectangular bar (127×32×12.7mm), as well as 1020 steel angle iron (203× side width 25 × wall thickness 4 mm) which provided a corner shape for the coating. The thickness of the ceramic coating was about 1.5-1.6 mm. The bond coat thicknesses were 0.28 mm and 0.5 mm for the angle iron specimens and the rectangular flat specimens, respectively.

Low Cycle and High Cycle Fatigue Tests

Low cycle and high cycle fatigue tests under simulated engine temperature and thermal stress conditions were conducted using a high power 1.5 KW CO_2 laser (EVERLASE, Coherent General Inc., Massachusetts). This test rig was controlled by a PC programmed to simulate different LCF and HCF temperature cycles. The pulsed laser mode for combined LCF and HCF tests, and the continuous wave (CW) mode for pure LCF tests, were used to generate the heating and cooling cycles. The specimen and experimental conditions for LCF and HCF tests are summarized in Table 1. In order to produce a spread beam with lower power density suitable for simulating diesel engine conditions, a Plano Concave ZeSe lens with focal length -330 mm was used. The specimen was placed at a distance 460 mm from the magnifying lens, the beam radius was increased from 7 mm to about 16 mm [11]. Because of the expanded Gaussian laser beam used, laser power density is expected to vary across the beam diameter. This beam profile can provide additional information on coating failure mechanisms associated with heat flux distributions. Laser power density distributions under test conditions are shown in Figure 1.

During the thermal fatigue testing, specimen surface temperatures were measured by two 8 micron infrared pyrometers (Model MX-M803 Maxline Infrared Thermometer Measurement and Control System, Ircon, Inc., Illinois), aimed at the beam center (giving the peak temperature) and 7 mm away from the center. The backside metal temperature was determined by a type-R thermocouple. The HCF combustion cycles were simulated using the pulsed laser mode, with total average beam power about 180 W. The laser pulse period was set at 92 milliseconds (ms), effective square wave equivalent pulse at about 6 ms. Because the high energy laser pulse was used, an HCF component was inherently superimposed to the LCF cycles. The temperature gradient across the coating system was achieved by backside air cooling.

Since the pyrometer (with response time > 25 ms) can not record the temperature swing generated by the pulsed laser, one dimensional (one-D) finite difference analysis has been used to model the thermal HCF temperature profile. The finite difference analysis method was compared with analytical solutions for both a uniform, constant irradiance model and a Gaussian beam model in calculating the surface temperature swing, so that the validity of the one dimensional finite difference analysis can be examined. In general, if beam diameter is larger than the characteristic depth $\sqrt{4\kappa\tau}$, where κ is the thermal diffusivity and τ the pulse width, a one-D

model will provide a reasonable estimate of the temperature distribution [13]. In the present study, the temperature swing predicted by all three approaches was essentially the same, implying that the Gaussian beam is sufficiently widespread to allow the use of the one-D assumption. Under the present HCF conditions, the HCF interaction depth where there is a noticeable temperature fluctuation (about 10% the surface temperature swing) is about 0.15 mm, as shown in Figure 2. Examples of the calculated stress distributions across the thermal barrier coating system on an angle iron under laser LCF and HCF testing conditions are shown in Figures 3 and 4, respectively [11]. It can be seen that during the initial heating stage, a steep compressive stress gradient is established in the ceramic coating. The temperature fluctuation induces high-frequency cyclic stresses on the coating surface. The dashed lines represent the ceramic surface stress values at the average steady state surface temperatures under the heat flux 0.323 MW/m^2.

Table 1. Laser thermal LCF and HCF tests under simulated engine cycling conditions

No	Material	Test type	Maximum surface temperature T_s,°C	Backside metal temperature T_m,°C	Heating/ cooling time min.	Total heating time hrs.	Total HCF cycles x10^6	Total LCF cycles	HCF cycles per LCF cycle, N^*_{HCF}
1	Angle iron TBC t_c*=1.6mm t_b†=0.28mm	LCF& HCF Pulse 180W	850	250	5/3	256	10	3067	3261
2	Angle iron TBC t_c=1.6mm t_b=0.28mm	LCF CW 180W	850	250	5/3	256	–	3067	–
3	Angle iron TBC t_c=1.6mm t_b=0.28mm	LCF& HCF Pulse 180W	850	250	30/5	256	10	510	19565
4	Angle iron TBC t_c=1.6mm t_b=0.28mm	LCF& HCF Pulse 180W	950	350	30/6	256	10	510	19565
5	Flat TBC t_c=1.5mm t_b=0.5mm	LCF& HCF Pulse 180W	920	250	30/5	153	6	307	19565
6	Flat TBC t_c=1.5mm t_b=0.5mm	LCF CW 180W	920	250	30/5	153	–	307	–

* Thickness of the ceramic coating.

† Thickness of the bond coat.

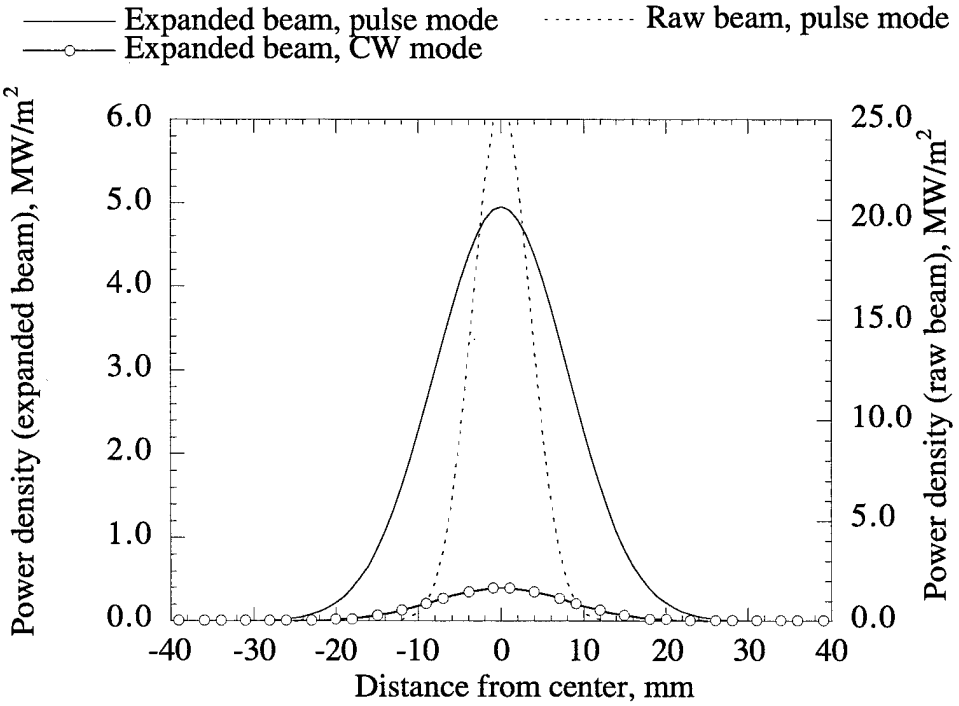

Fig. 1 Laser power density distributions estimated from the measured laser waveform and total power output [11] . The peak power density from the pulsed laser beam at the beam center is 4.95 MW/m^2, corresponding to the average or equivalent CW laser power density 0.323 MW/m^2. Minor beam non-uniformity observed is neglected.

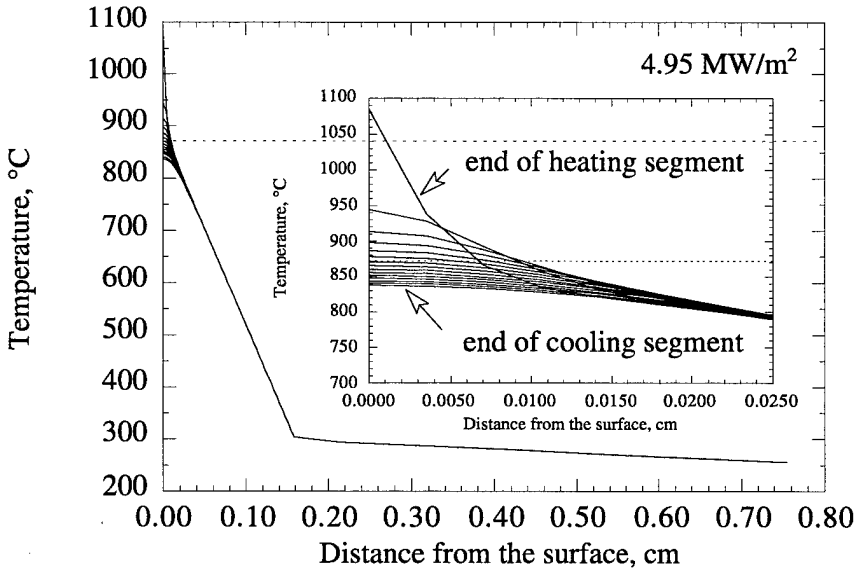

Fig. 2 Temperature profiles generated in the beam center direction in the thermal barrier coating system by pulsed laser heating (pulse width 6 ms). Ceramic coating thickness 1.6 mm.

Microscopic Examinations

The tested coating surfaces and cross-sections were examined under both optical and electron scanning microscopes to obtain information on crack density and distribution, as well as crack surface morphology. In order to prevent damage by specimen cross-section preparation, a pressurized epoxy infiltration method for specimen mounting has been used. By this technique, epoxy was first poured over specimens and their holding cups in a vacuum chamber. After the epoxy degassing in vacuum, the specimens were moved into a pressurized chamber (up to 8.3 MPa) for 24 hours, as the epoxy cured. Therefore, the epoxy fills the cracks in the specimen, and the original crack characteristics generated in thermal fatigue tests are preserved.

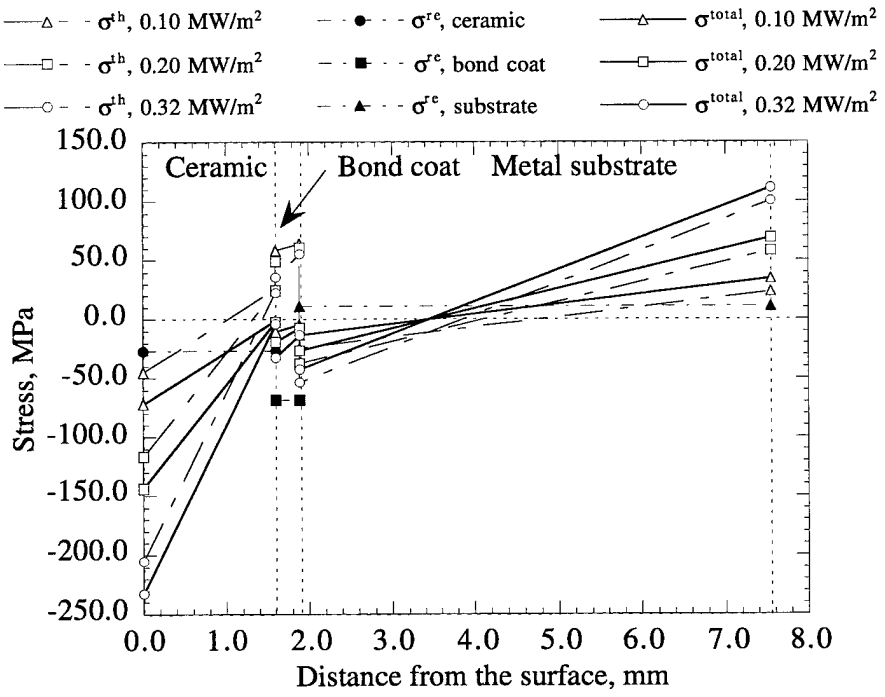

Fig. 3 Stress distributions in a thermal barrier coating system on an angle iron at steady state heating for various heat fluxes (LCF or HCF conditions). σ^{th}, σ^{re} and σ^{total} are thermal stresses, residual stresses and total stresses in the coating system, respectively.

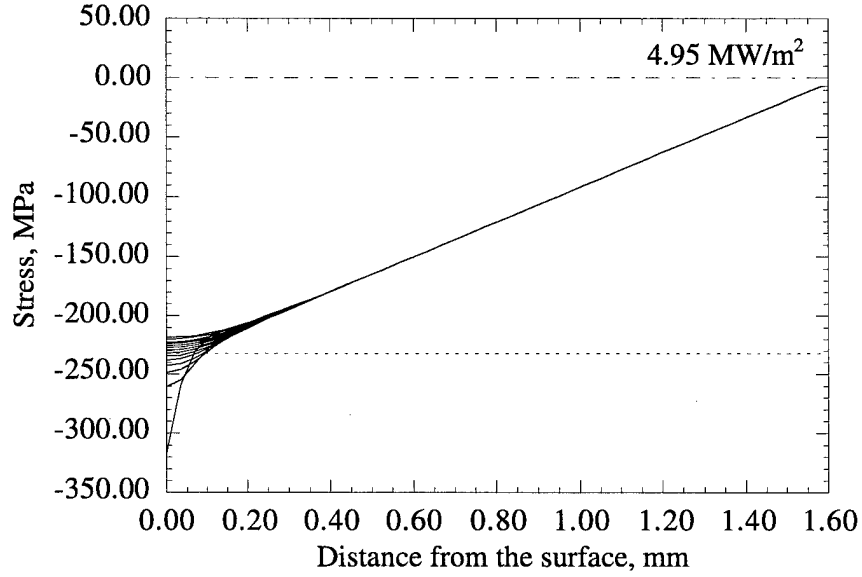

(a)

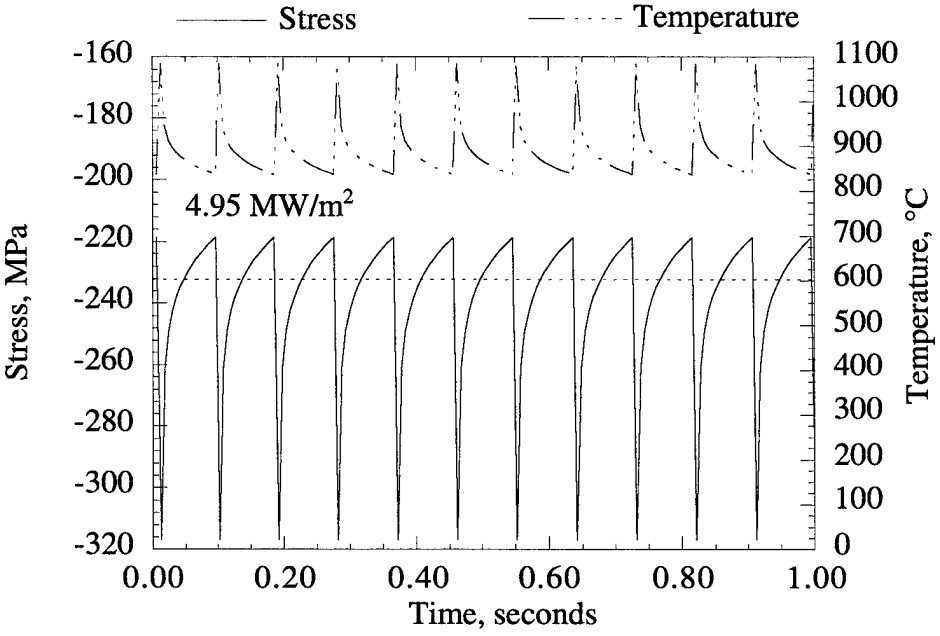

(b)

Fig. 4 Calculated thermal stresses induced by pulsed laser heating under HCF conditions. Besides a constant stress gradient generated by the steady state heating, high frequency HCF cyclic stresses are present near the ceramic coating surface. Laser peak power density 4.95 MW/m^2. (a) Stress distributions in the thermal barrier coating; (b) Thermal HCF stress history at the ceramic surface.

Thermal Shock Tests

In order to investigate the pure HCF component on crack propagation, laser thermal shock tests on coating surfaces were conducted. The specimen configuration is illustrated in Figure 5. During the test, two specimens were clamped together with the two pre-polished side surfaces in contact. The ceramic surface and metal substrate temperatures were monitored and recorded by pyrometer and thermocouple, respectively. The laser power was set at 1600 or 900 W, and laser pulse heating time of 100 ms. These laser test conditions generated maximum surface temperature swings of about 750°C and 420°C, with an HCF interaction depth of about 0.3 mm. The cooling times between each heating cycle were chosen as 1 minute and 0.5 minute for 1600 W and 900 W tests, respectively. The sufficient cooling time allowed the specimen substrate temperature to remain below 35°C throughout the testing. After a prescribed number of thermal shock cycles, the specimens were unclamped and the cross-sections were carefully examined under an optical microscope. The crack lengths in the ceramic coating were also measured periodically up to 5000 cycles. Because the thermal loads act only on the coating surface, this experiment can completely eliminate LCF influence, and thus providing information on HCF failure modes under severe and accelerated HCF conditions.

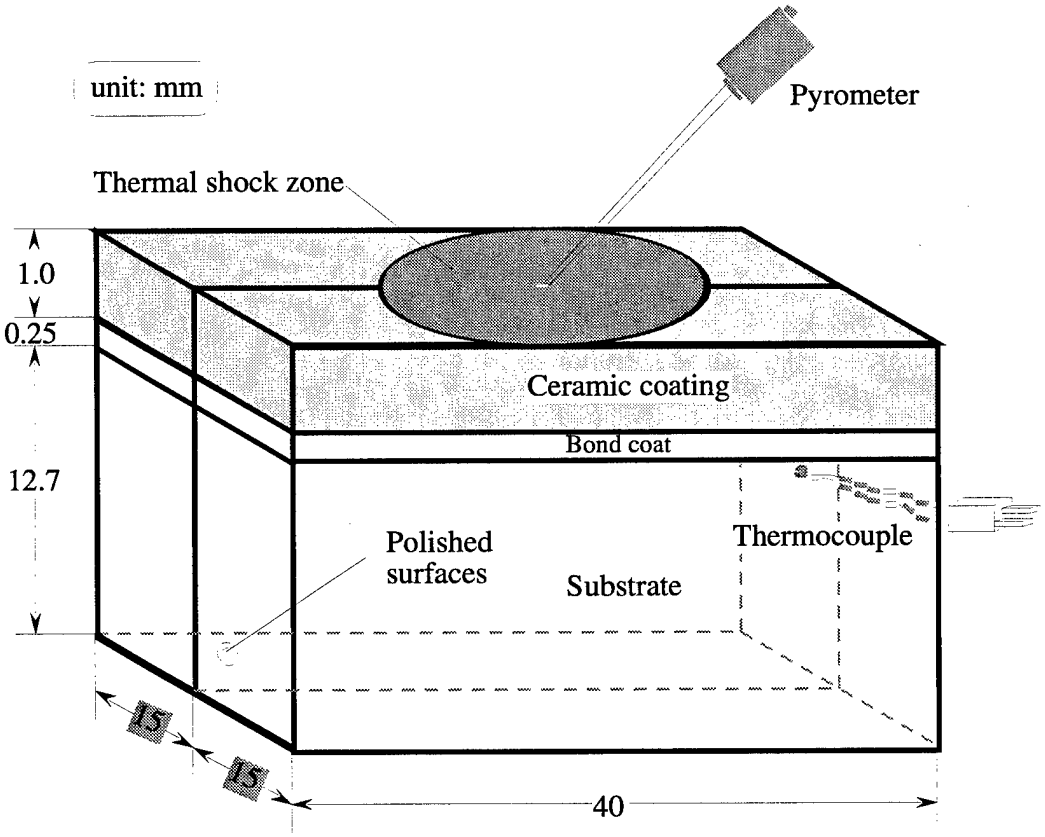

Fig. 5 Schematic diagram showing specimen configuration for laser thermal shock tests.

EXPERIMENTAL RESULTS

Ceramic Coating Failure Modes under Laser Simulated Engine Conditions

The crack patterns on the angle iron and flat specimen surfaces are schematically illustrated in Figure 6. At the angle iron corners, nearly parallel cracks which run across the corners were formed by the laser thermal fatigue tests. In contrast, equiaxial crack networks (mud flat cracks) were generated by the laser beam on the flat specimen surfaces. However, at the edges of the flat specimens, parallel cracks similar to those found on the angle iron corners were observed with crack direction perpendicular to the edges. Compared to pure LCF tests, the combined LCF and HCF initiated more secondary cracks, and micro-spallation at the cracked surfaces. In general, surface crack density and crack width increase towards the beam center, and thus increase with laser power density. The optical and SEM micrographs of the cracked surfaces of the specimens are shown in Figure 7 (a) to (d). The results suggest that much higher surface stresses were induced at the ceramic surface by the addition of the pulsed laser HCF component. The pure LCF tested specimens have relatively intact coating surfaces, and the thermal fatigue cracks are relatively regular with well matched crack faces. However, the combined LCF and HCF tests produced more severe coating surface damage. Besides the major thermal fatigue cracks, surface coating micro-spallation, crack branching and loosened particle intrusion into the cracks were observed. For all combined LCF and HCF tested specimens, the specimen with the 30 minute heating/5 minute cooling cycles at lower temperature (T_s=850°C) showed the least surface damage. In contrast, the most severe surface damage was found for the specimen with the 30 minute heating/5 minute cooling cycles at the higher temperature (T_s=950°C). In the latter specimen, cracks were branched into multiple crack networks and accompanied with more coating spallation, and the major crack density and the crack width were also significantly higher.

Examination of the cross-sections of the failed coating systems, after laser thermal fatigue testing, has further confirmed the experimental observation from the surfaces. As shown in Figure 8, the combined LCF and HCF tested coating has generated severe surface damage, as compared to the LCF tested coating. In addition, the coating cracks developed under HCF conditions induced many lateral subcracks. This crack branching phenomenon could result in multiple delaminations of the coating under the subsequent HCF loading. It can also be noted that cracks generated in the ceramic coatings by laser LCF and/or HCF experiments possess a wedge-shape nature, with the largest opening at the coating surfaces. The crack displacement gradient is coincidentally consistent with the compressive stress gradient and the temperature gradient in the coating at temperature.

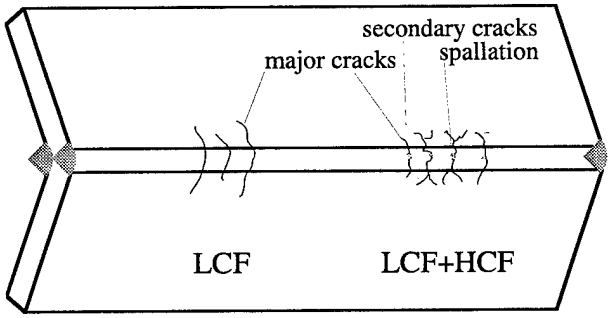

(a) Angle iron specimen

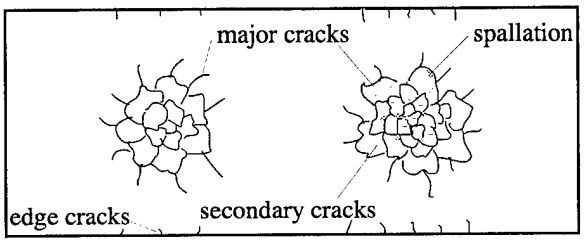

(b) Rectangular flat specimen

Fig. 6 Schematic diagram showing the crack patterns on coating surfaces after laser testing.

Crack Propagation Kinetics

Surface crack growth rates for the angle iron specimen, under various test conditions, have been determined by measuring various crack lengths observed in single specimens after each test. Statistical analysis has been used to compare these results, as shown in Figure 9. Under the present testing conditions, the total crack length in the ceramic coating system increases with LCF cycle number. Higher surface temperature results in a longer crack length. Even though the differences between the major crack lengths (measured from the primary cracks perpendicular to the coating surface) under HCF and LCF test conditions (No.1 and No.2 tests in Table 1) are not so significant, the HCF component tends to increase the overall coating crack length especially when crack branching is considered. However, from the crack propagation rates plotted in Figure 10, it can be seen that significant LCF and HCF interactions exist during the thermal fatigue tests. The crack tip branching effect in test No.2 has been illustrated in the hatched area in Figure 10 (a). It seems that the fatigue crack growth rate in the ceramic coating strongly depends on the characteristic HCF cycle number, N^*_{HCF}, which is defined as HCF cycle numbers per LCF cycle. From Figure 10 (b), it can be seen that, the crack growth rate is increased from 0.36 μm/LCF cycle for a pure LCF test (N^*_{HCF}=0) to 1.8 μm/LCF cycle for a combined LCF and HCF test (N^*_{HCF} =20,000), when the maximum surface temperature T_s is 850°C. The crack growth rate is approximately 2.8 μm/LCF cycle when the maximum surface temperature T_s is 950°C.

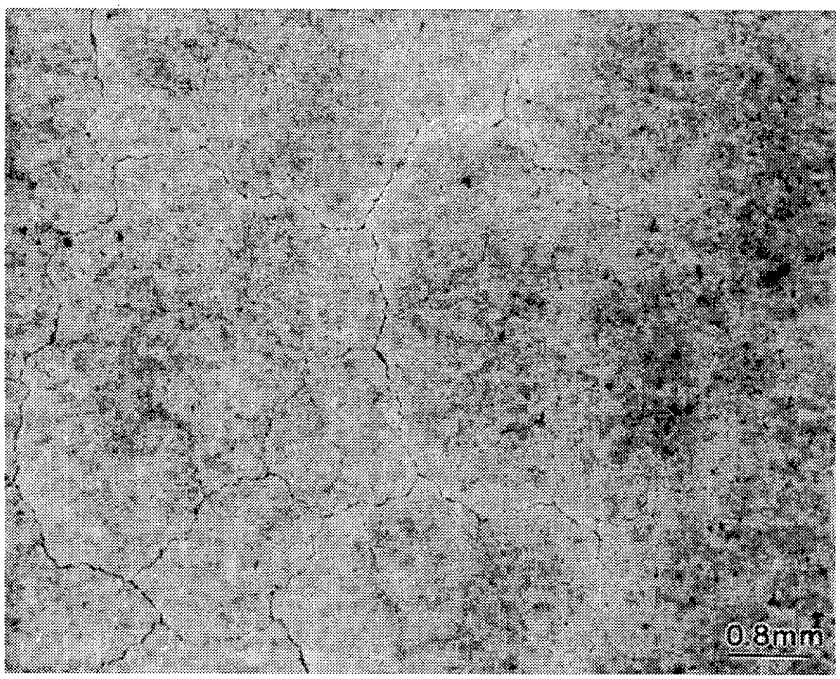

(a)

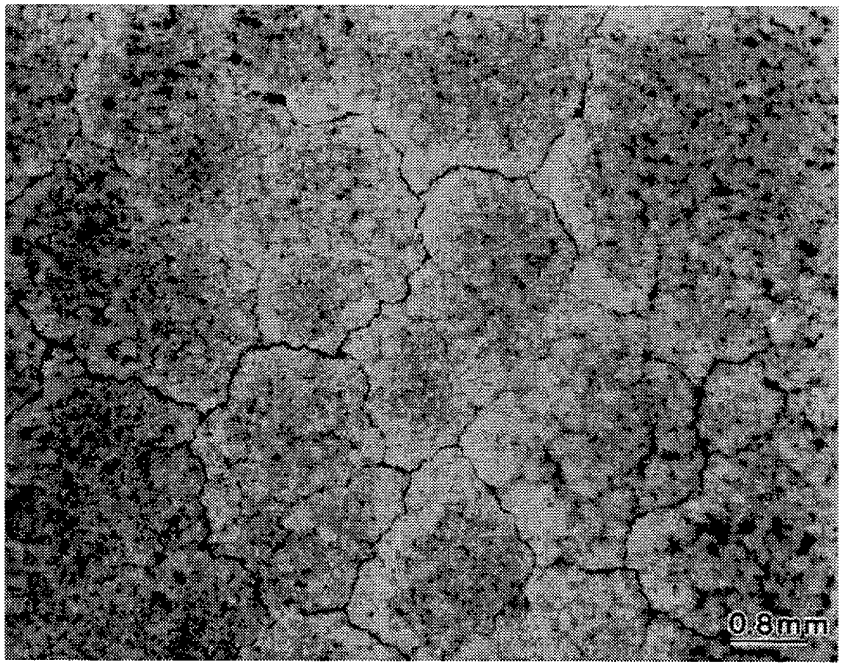

(b)

Fig. 7 Optical micrographs of ceramic coating surfaces of the flat specimens after the laser thermal fatigue testing (T_s=920°C). (a) LCF tested, after total 153 hours heating and 307 LCF cycles; (b) Combined LCF abd HCF tested, after total 153 hours heating, 307 LCF cycles and 6×10^6 HCF cycles.

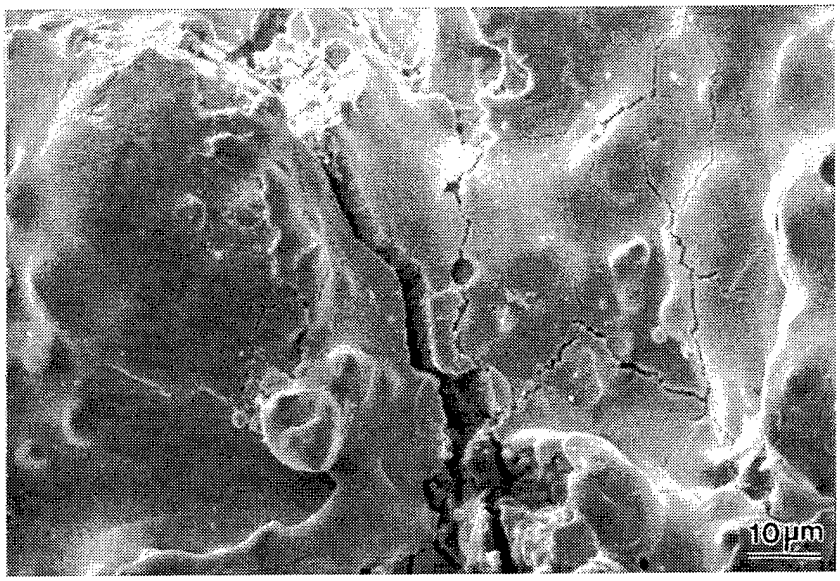

(c)

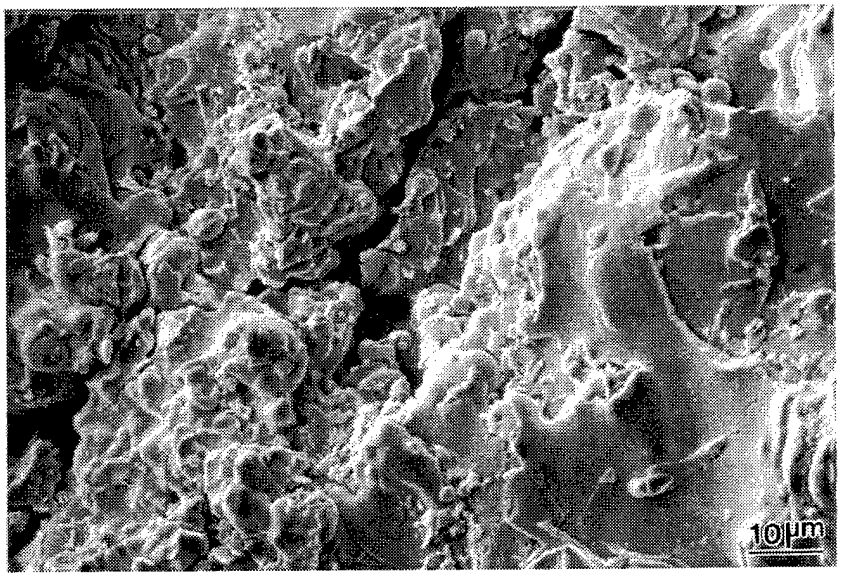

(d)

Fig. 7 Continued. SEM micrographs of ceramic coating surfaces of the angle iron specimens after the laser thermal fatigue testing (T_s=850°C, 5 minute heating and 3 minute cooling cycles). (c) LCF tested, after total 256 hours heating and 3067 LCF cycles; (d) Combined LCF and HCF tested, after total 256 hours heating, 3067 LCF cycles and 10×10^6 HCF cycles.

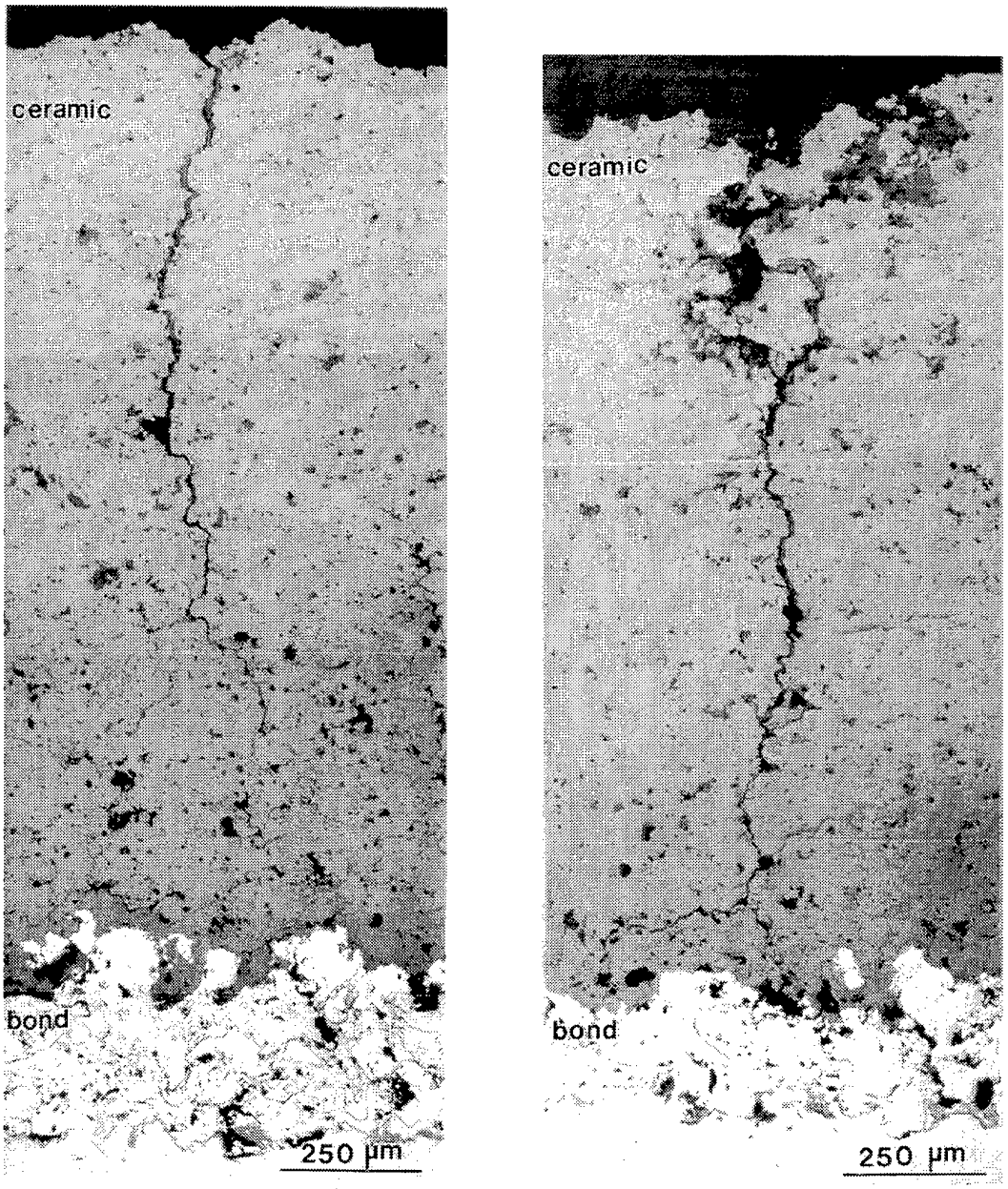

(a) (b)

'Fig. 8 Optical micrographs of the cross-sections of the ceramic coatings on the angle irons after the laser thermal fatigue testing (30 minute heating and 5 to 6 minute cooling cycles). (a) LCF tested, after total 256 hours heating and 510 LCF cycles, T_s=850°C; (b) Combined LCF and HCF tested, after total 256 hours heating, 510 LCF cycles and 10×10^6 HCF cycles, T_s=950°C.

Crack Growth under Thermal Shock Tests

Figure 11 illustrates the crack growth kinetics under laser thermal shock conditions. It can be seen that higher temperature swing results in faster crack growth rate. The cracks initiated and extended rapidly during the initial stage, then grew in a much slower rate. Although the thermal loading was acting only on the surface layer, the cracks propagated continuously, deep into the coating. These experiments demonstrate the even shallow surface thermal cyclic loading can cause not only surface crack initiation but also propagation. In fact, some of the cracks have reached near the ceramic/bond coat interface after 5000 cycles, when surface temperature swing was about 700°C. A typical micrograph of a specimen cross-section showing crack morphology induced by thermal shock tests is shown in Figure 12.

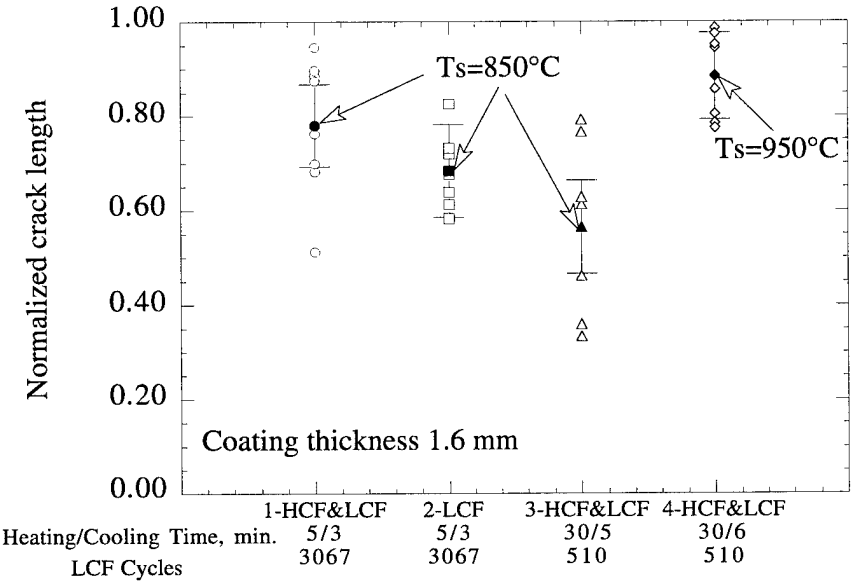

Fig. 9 Thermal fatigue crack lengths measured in thermal barrier coatings after laser LCF and HCF testing. Experimental data with Bonferroni multiple range analysis (95% confidence), significant difference detected between tests 1 and 3, 2 and 4, and 3 and 4. Total heating time 256 hours, total HCF cycles 10 million for combined LCF and HCF tests.

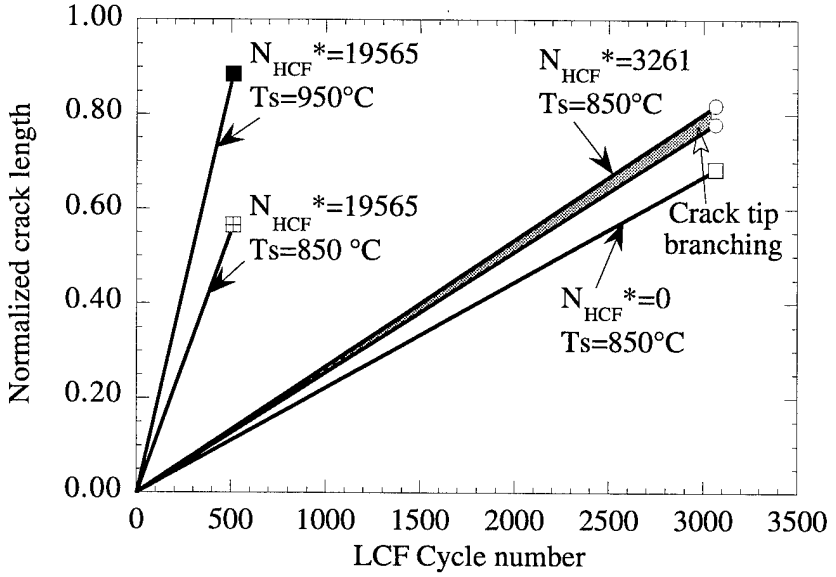

(a)

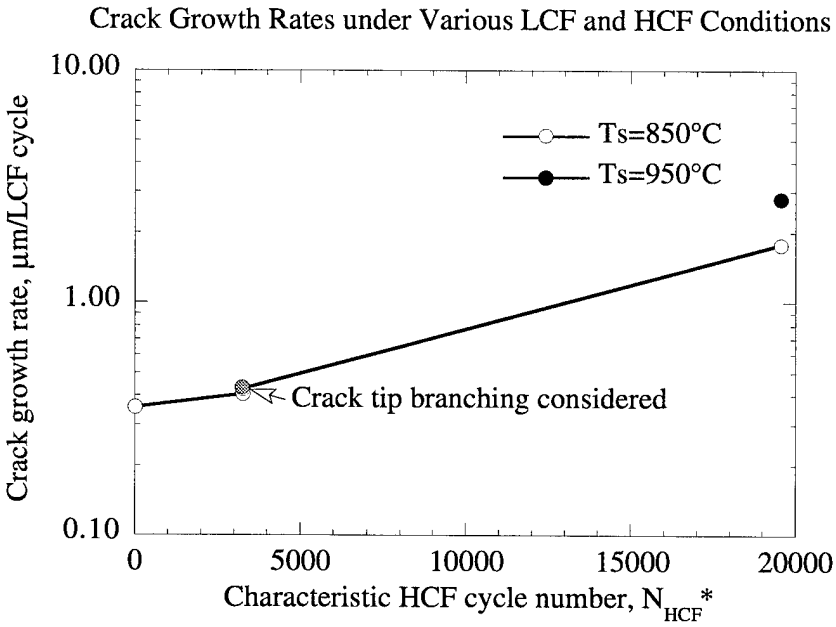

(b)

Fig. 10 Fatigue crack propagation kinetics. Ceramic coating thickness 1.6 mm, total heating time 256 hours, and total HCF cycles 10 million for combined LCF and HCF tests. (a) The crack length (normalized to coating thickness) as a function of LCF cycle number; and (b) Crack growth rate as a function of characteristic HCF cycle number, N^*_{HCF}.

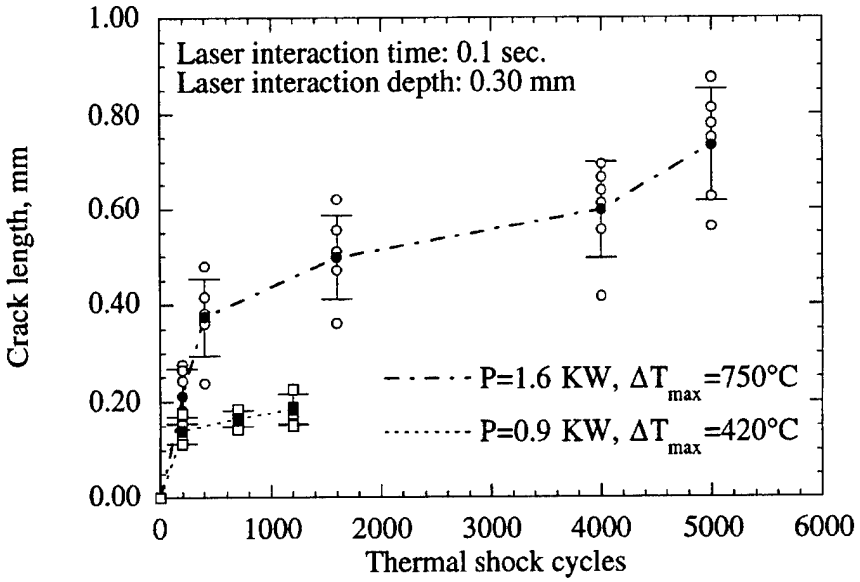

Fig. 11 The crack propagation rates as a function of thermal shock cycles. Ceramic coating thickness 1.0 mm.

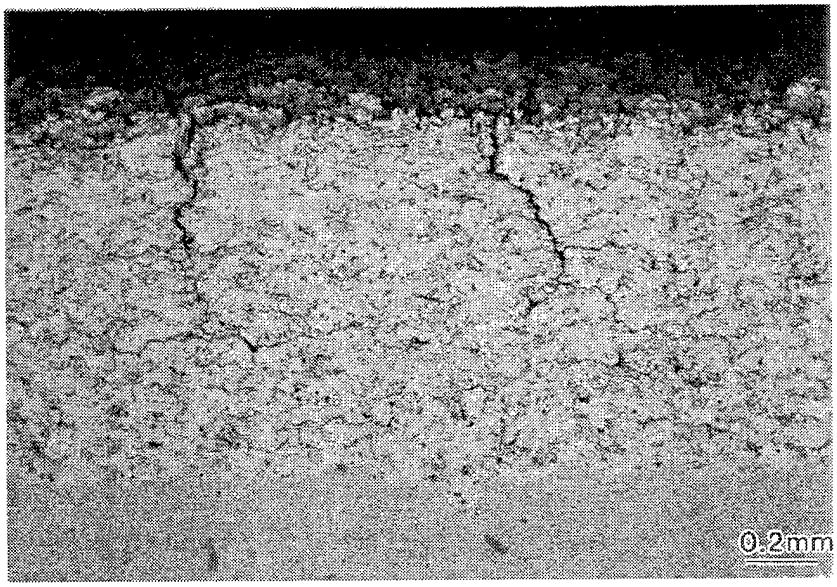

Fig. 12 SEM micrograph of a specimen cross-section showing crack morphology induced by thermal shock tests. The coating experienced 5000 thermal shock cycles at the maximum temperature swing of 750°C.

DISCUSSION

Crack Initiation During Thermal Fatigue Tests

The plasma sprayed ZrO_2-Y_2O_3 ceramic coatings contain microcrack networks with a typical crack width around 0.5-1 μm after processing. Therefore, initiation of larger cracks at the coating surface during thermal fatigue testing will not be a difficult process. The mechanisms of the crack initiation can be high peak compressive stress induced cracking at the heating stage (especially under combined LCF and HCF conditions), and surface tensile stress induced cracking during cooling. The surface tensile stresses, mainly generated by coating shrinkage due to the coating sintering and creep at temperatures, are detrimental to coating thermal fatigue properties [11].

During thermal fatigue testing, ceramic sintering and creep will occur under the given temperature and stress conditions. Due to the porous and microcracked nature of plasma-sprayed ceramic coatings, the primary creep stage is often observed for these coatings, with the strain rate continuously decreasing with time [11, 14]. This creep behavior is related to a stress-enhanced ceramic sintering phenomenon, as has been observed in experiments [15]. At lower temperatures, the relative boundary sliding of plasma-sprayed splats and grains, and the stress redistribution around the splats and microcracks are probably important mechanisms for ceramic creep deformation. This stress-dependent deformation will lead to coating shrinkage and thus stress relaxation at temperature under the compressive stresses. An example of the stress distribution profiles in the coating, as shown in Figure 13, dictates this stress relaxation process.

For a given heat flux, the HCF mode will generate a much faster creep rate near the coating surface compared to the pure LCF mode because of the large temperature fluctuation. Using the literature reported creep data for the plasma sprayed coating [16], this phenomenon has been modeled in the present study, as shown Figure 14. The instantaneous, incremental creep strain is much higher under the superimposed HCF condition compared with the LCF mode, consequently resulting in a higher total creep strain in the coating. Since the laser HCF component will promote both the coating surface creep and the coating surface compressive cracking, the accelerated crack initiation and higher surface crack density at the coating surfaces are expected, as has been confirmed by this experiment.

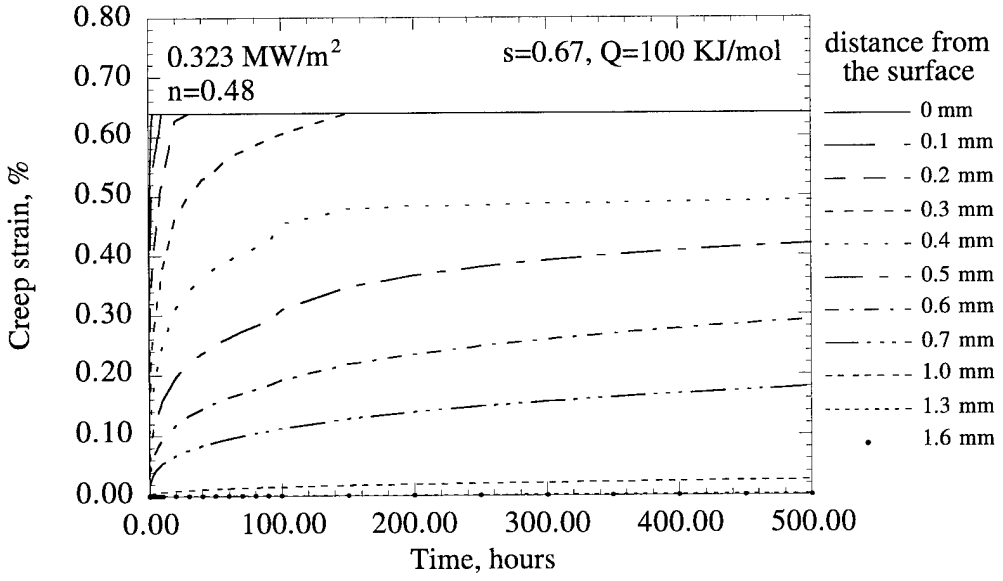

(a)

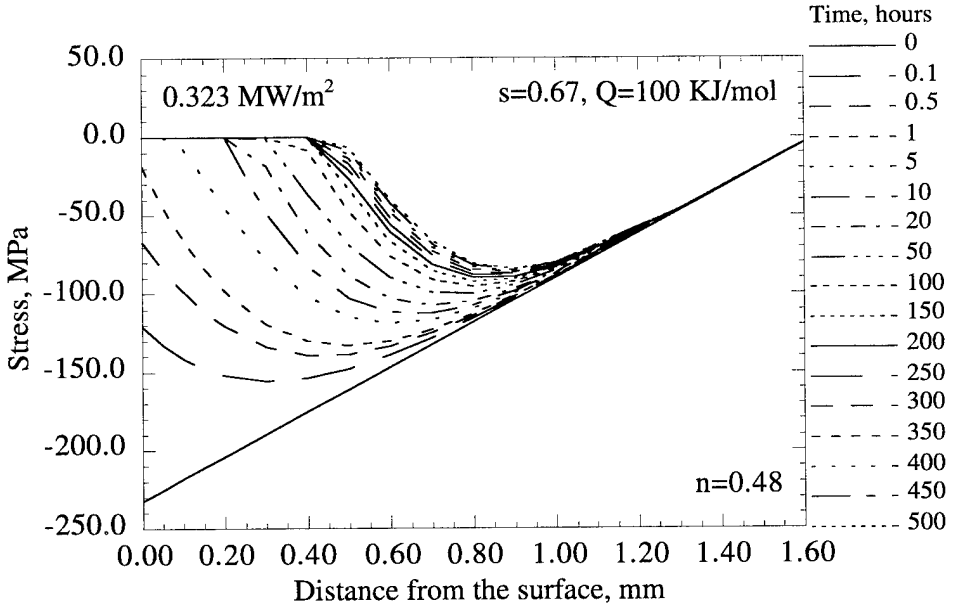

(b)

Fig. 13 Calculated creep strains and stress relaxation in the ceramic coating as a function of time. Heat flux is 0.323 MW/m^2. The stress exponent n , time exponent s and activation energy Q are listed in the Figure [11].

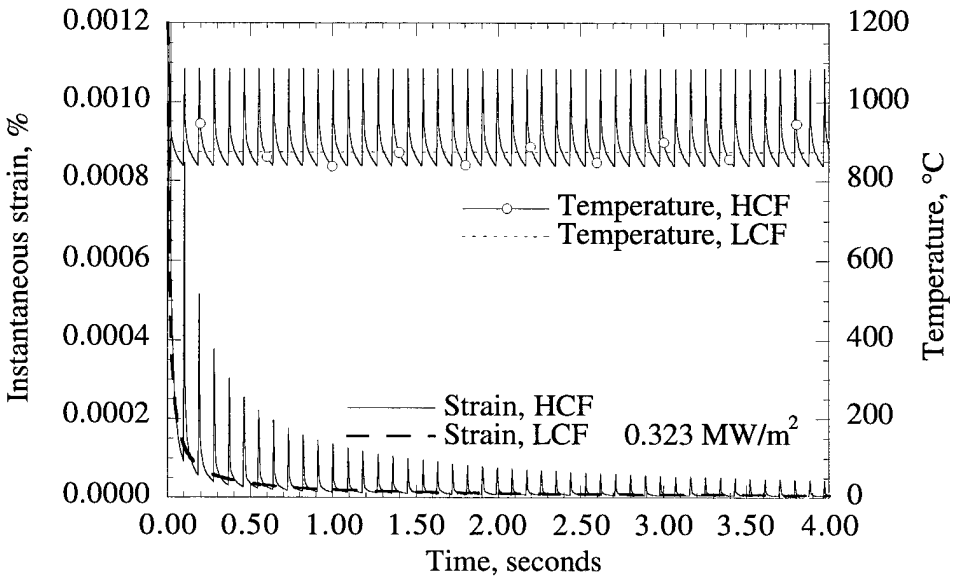

(a)

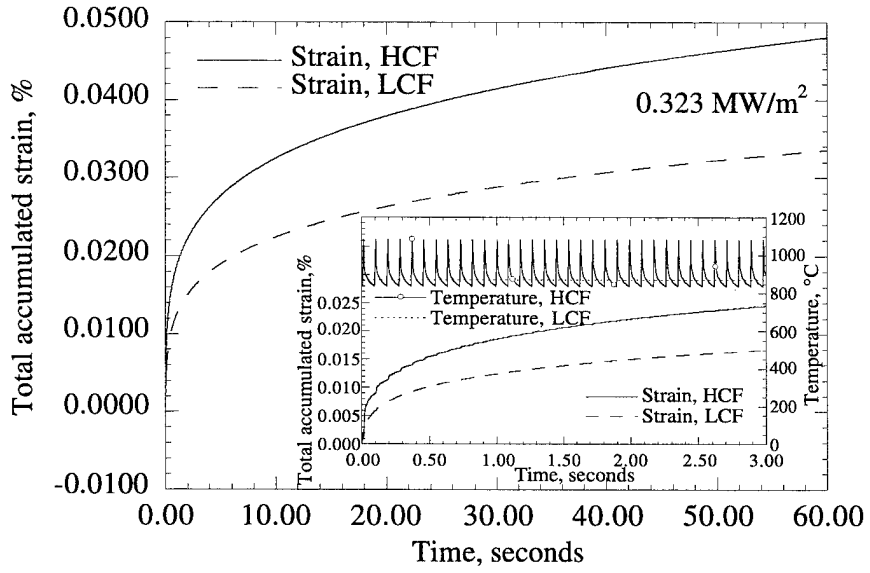

(b)

Fig. 14 Predicted instantaneous, incremental creep strains and total accumulated strains under LCF and HCF conditions from the literature reported ceramic creep data showing that HCF component significantly increases the coating creep strains. Heat flux is 0.323 MW/m^2. The stress exponent n =0.48, time exponent s=0.82 and activation energy Q=114 KJ/mol. (a) Instantaneous creep strains; (b) Total accumulated strains.

During a superimposed thermal LCF and HCF testing, the surface vertical crack growth can be generally induced by both LCF and HCF components, as illustrated in Figure 15. The crack growth rate with respect to LCF cycle number can be expressed as[11]

$$\left(\frac{da}{dN}\right)_{LCF} = C_1\left(\Delta K_{LCF}\right)^q + \int_0^{N^*_{HCF}} C_2\left(\Delta K_{HCF}\right)^q dN_{HCF} \qquad (1)$$

where q, C_1 and C_2 are constants, ΔK_{LCF} and ΔK_{HCF} are stress intensity factors of the crack under low cycle and high cycle loads, respectively. The stress intensity factors are functions of crack length and stress magnitudes and distributions. The term, N^*_{HCF} is the characteristic HCF cycle number, defined as HCF numbers per LCF cycle.

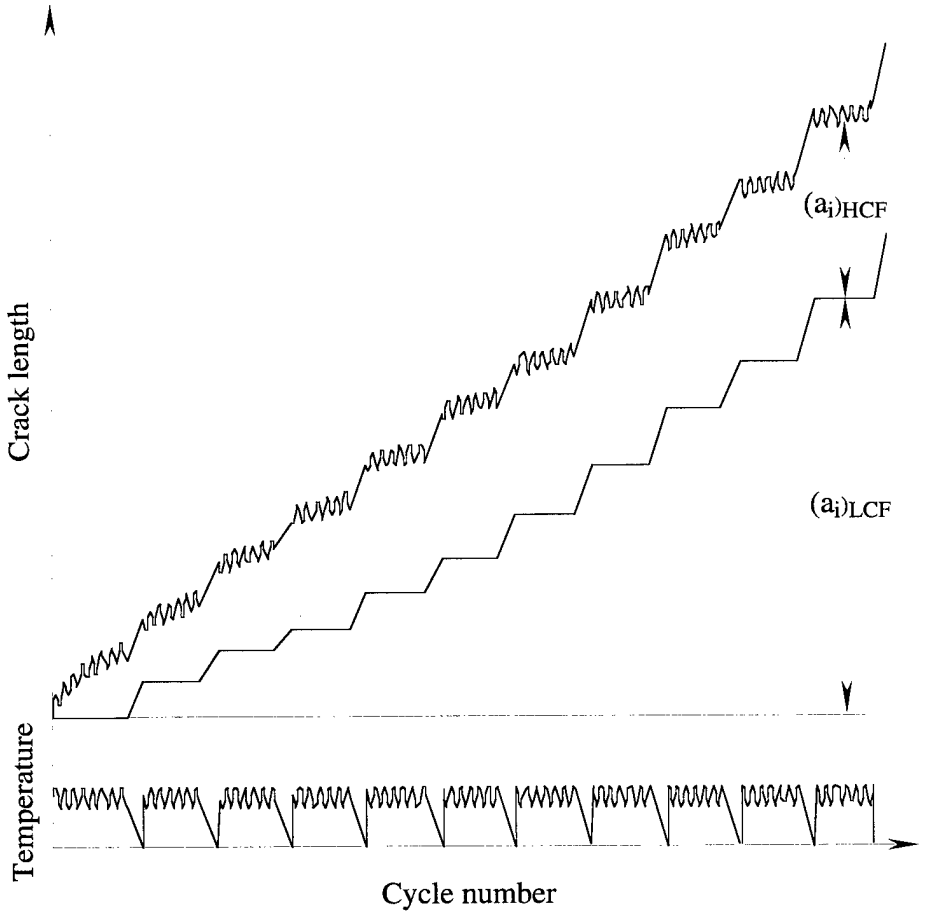

Fig. 15 Schematic diagram showing crack growth resulting from thermal LCF and HCF loads.

Under the conditions that the oxidation of the bond coat and the substrate is not important, the low cycle fatigue mechanism is primarily associated with coating sintering and creep at high temperatures. The creep in the ceramic coating will induce a tensile stress state during cooling, resulting in the crack growth under cyclic conditions, as schematically shown in Fig 16. The LCF stress distributions as a function of time and coating layer depth are illustrated in Figure 17. The mode I stress intensity amplitude for LCF crack growth can be written as

$$\Delta K_{1LCF} = Y \cdot \left[\sigma_{LCF} - \sigma_{th}\right] \cdot \sqrt{\pi a(i)} \tag{2a}$$

and

$$\sigma_{LCF} = \int_0^{t_i} \dot{\varepsilon}_p(\sigma_{th}, T, t)dt \cdot \frac{E_c}{1 - \nu_c} \tag{2b}$$

where Y is a geometry factor associated with the crack configuration, σ_{LCF} and σ_{th} are the in-plane LCF stress upon cooling and the in-plane thermal stress at temperature respectively, $\dot{\varepsilon}_p(\sigma_{th}, T, t)$ is the strain rate resulting from ceramic creep, T is temperature, t_i and $a(i)$ are the total heating time and crack length at the ith cycle, E_c and ν_c are the Young's modulus and Poisson's ratio of the ceramic coating, respectively.

The high cycle fatigue is associated with the cyclic stresses that originated from the high frequency temperature fluctuation at the ceramic coating surface. Because this temperature swing results in a significant thermal strains, considerable stresses will develop at the coating surface. HCF stresses are dynamic in nature with a very short interaction time; therefore, stress relaxation can be neglected. With a surface crack in the coating, the HCF thermal loads can be equivalently acting on the crack by a wedging process, as schematically illustrated in Figure 18. This wedging process, which provides an intrinsic mechanism for the HCF phenomenon, can be further enhanced by crack face shifting and spalled particle intruding [11]. The bending moments resulting from the HCF cyclic stresses will also cause multiple delaminations of the coating. The net mode I stress intensity factor amplitude for this case can be expressed as [17]

$$\Delta K_{1HCF} = \frac{2 \cdot P}{\pi} \frac{1 + f(i)}{\sqrt{a(i)^2 - b_i^2}} \sqrt{\pi \cdot a(i)} \tag{3a}$$

and

$$P = \sigma_{HCF} \cdot b_i \tag{3b}$$

where P is a concentrated load per unit thickness acting on the crack, and σ_{HCF} is the HCF stress, b_i is the load acting distance from the surface which is taken as laser interaction depth in the

present study. $f(i)$ is a geometry factor, which can be related to the crack length $a(i)$ and the acting depth b_i in the following form [17]

$$f(i)=\left[1-\left(\frac{b_i}{a(i)}\right)^2\right]\cdot\left[0.2945-0.3912\cdot\left(\frac{b_i}{a(i)}\right)^2+0.7685\cdot\left(\frac{b_i}{a(i)}\right)^4\right.$$

$$\left.-0.9942\cdot\left(\frac{b_i}{a(i)}\right)^6+0.5094\cdot\left(\frac{b_i}{a(i)}\right)^8\right] \tag{4}$$

Figures 19-22 illustrate the relationship between the stress intensity factor amplitude and the normalized crack length, with various values of b_i, ΔT, α_c and E_c of the coating. In general, the stress intensity factor induced from the HCF loads has the highest values when the crack is relatively small (the normalized crack length below 1), then decreases as the crack grows and approaches the interface. The HCF damage effect will increase with heat flux (thus with the temperature swing), the thermal expansion coefficient and elastic modulus of the ceramic coating, as well as with the HCF interaction depth. The proposed HCF mechanism is consistent with experimental observations from thermal fatigue tests and thermal shock tests.

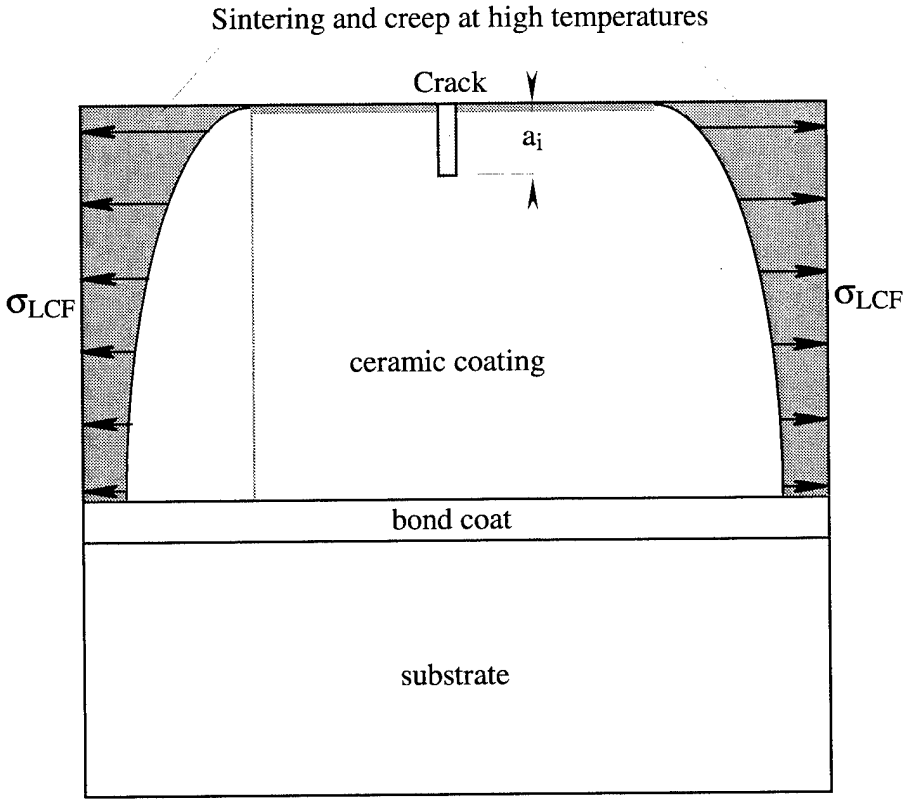

Fig. 16 Ceramic sintering and creep result in non-elastic strains (shown in shadowed area) at temperature, thus generating tensile stresses upon cooling.

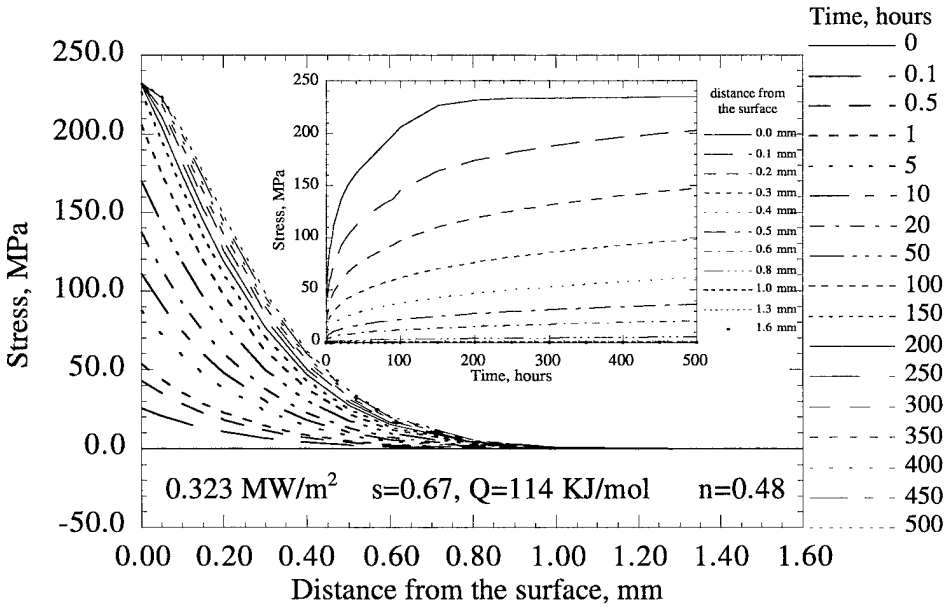

Fig. 17 Tensile stresses are generated in the ceramic coating during cooling as a function of time and coating layer depth. These stresses are considered as a primary mechanism for LCF crack growth.

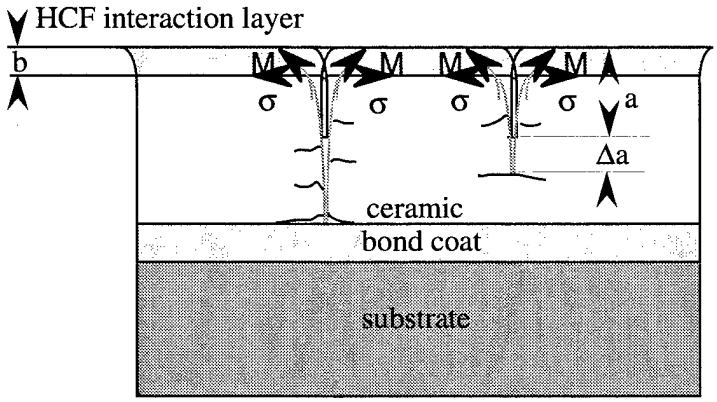

(a) crack growth under HCF conditions by surface wedging mechanism

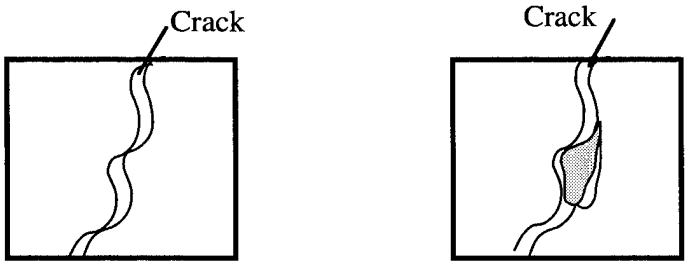

(b) enhanced surface wedging damage by surface crack face shifting

(c) enhanced surface wedging damage by spalled particle intruding

Fig. 18 Schematic diagram illustrating surface wedging mechanism during high cycle fatigue process.

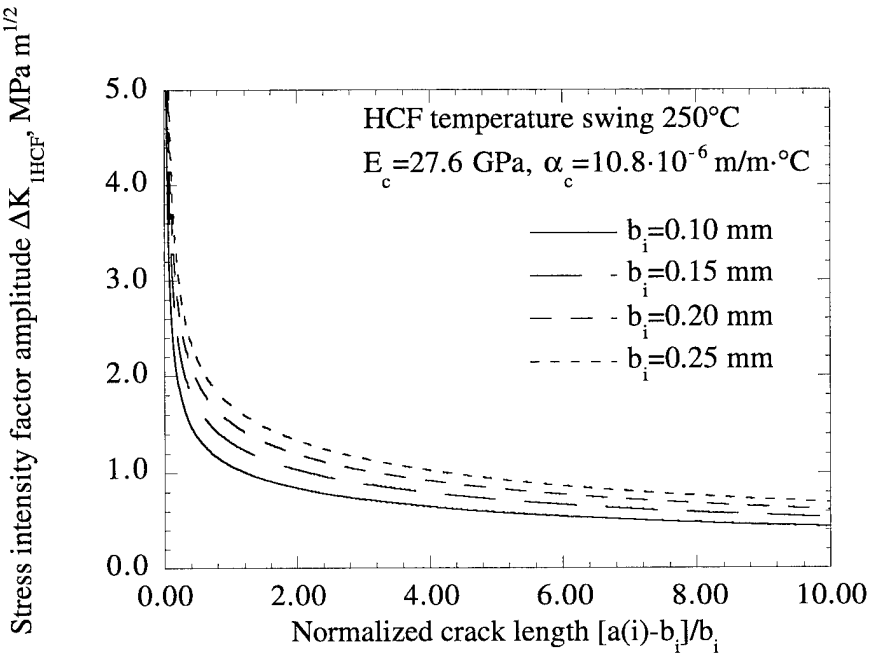

Fig. 19 The relationship between the stress intensity factor amplitude and the laser interacting depth b_i as a function of the normalized crack length.

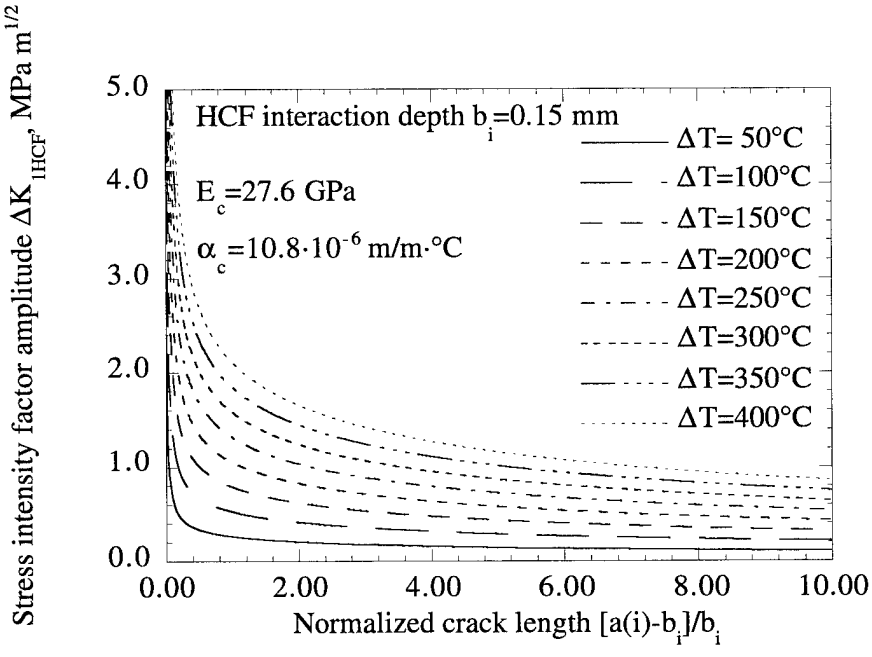

Fig. 20 The relationship between the stress intensity factor amplitude and the temperature swing ΔT as a function of the normalized crack length.

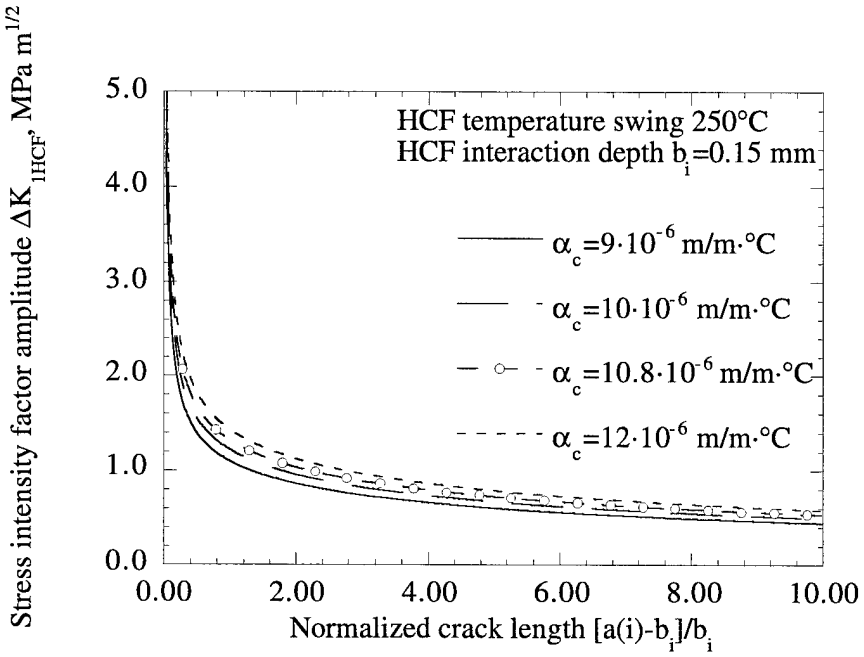

Fig. 21 The relationship between the stress intensity factor amplitude and the thermal expansion coefficient α_c of the coating as a function of the normalized crack length.

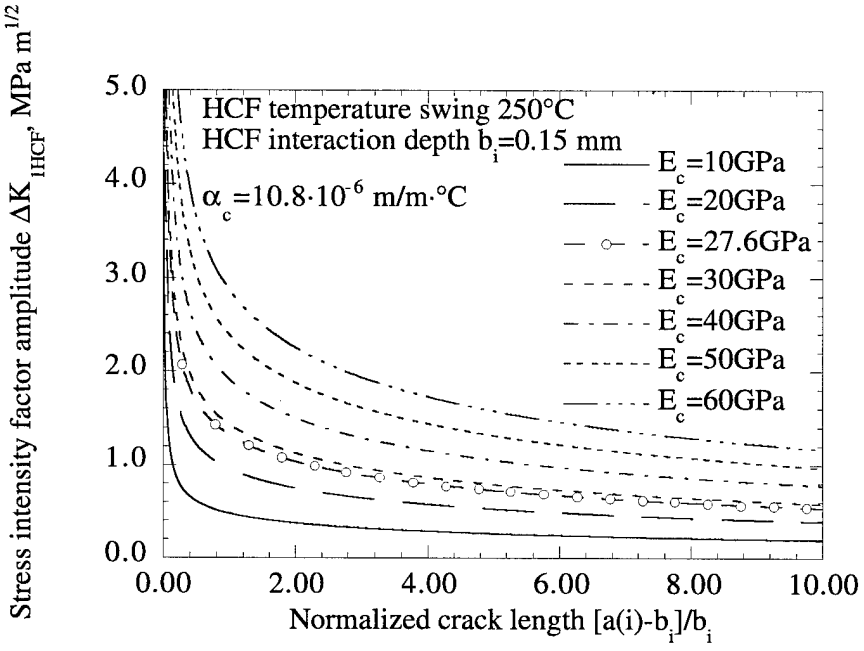

Fig. 22 The relationship between the stress intensity factor amplitude and the elastic modulus E_c of the coating as a function of the normalized crack length.

The Interactions between LCF and HCF Crack Growth

Strong interactions between LCF and HCF have been observed from the experiments. The high cycle fatigue component promotes surface crack initiation and increases surface crack densities. This causes fast initial crack propagation near the coating surface according to the surface wedging mechanism, because of the extremely high stress intensity values at the initial stage. The longer cracks then increase subsequent LCF stress intensity amplitudes, thus leading to a faster crack growth rate under LCF mechanism. According to Equation (1), the HCF component equivalently increases the effective stress intensity at a given LCF cycle. As a consequence, the crack growth rate increases with increasing characteristic HCF cycle number. The LCF component will accelerate the subsequent HCF crack growth at high temperatures by predominantly two mechanisms. Stress relaxation at high temperatures can significantly reduce the effective compressive stresses in the coating;.coating surface sintering under LCF cycles could considerably increase the coating elastic modulus. Both processes will lead to greater HCF damage to the coating.

CONCLUSIONS

1. In the absence of severe interfacial oxidation, the LCF mechanism is closely related to coating sintering and creep phenomena at high temperatures. The HCF mechanism, however, is associated with the surface wedging process. The HCF damaging effect will increase with the temperature swing, the thermal expansion coefficient and elastic modulus of the ceramic coating, as well as with the HCF interaction depth.

2. Experiments have shown strong interactions between LCF and HCF processes. The combined LCF and HCF tests induced more severe coating damage compared to the pure LCF test. The fatigue crack growth rate in the ceramic coating strongly depends on the characteristic HCF cycle number, N^*_{HCF}, which is defined as HCF cycle number per LCF cycle. The crack growth rate is increased from 0.36 μm/LCF cycle for a pure LCF test to 2.8 μm/LCF cycle for a combined LCF and HCF test at N^*_{HCF} about 20,000.

ACKNOWLEDGMENTS

This work was performed while the first author held a National Research Council - NASA Lewis Research Center Research Associateship partially supported by the Army Research Laboratory at the NASA Lewis Research Center. The authors are indebted to M. Brad Beardsley, Caterpillar Inc., for valuable discussions. The authors are grateful to George W. Leissler and Sandra L. Skotko for their assistance in the preparation of TBC coatings and metallographic specimens, and to Dennis L. Weismantel for his assistance in the laser waveform measurement and related data acquisition.

REFERENCES

[1] Miller, R. A., "*Assessment of Fundamental Materials Needs for Thick Thermal Barrier Coatings for Truck Diesel Engines*", *NASA TM-103130, DOE/NASA/21794-1*, 1990.

[2] Yonushonis, T. M., "*Thick Thermal Barrier Coatings for Diesel Components*", *NASA CR-187111*, 1991.

[3] Morel, T., "*Analysis of Heat Transfer in LHR Engines: A. Methodology, Validation, Applications; B. Translucence Effects in Ceramics*", in *Proceedings of the 1987 Coatings for Advanced Heat Engines Workshop* (eds. Fairbanks, J.), II17-II28, Castine, Maine, July 27-30, 1987.

[4] Dickey, D., Vinyard, S., Callahan, T. and Keribar, R., "*The Effect of Insulated Diesel Surfaces on Performance, Emissions and Combustion*", in *Proceedings of the Twenty-Fifth Automotive Technology Development Contractors' Coordination Meeting* 49-56, **P209**, Dearborn, Michigan, October 26-29, 1988.

[5] Beardsley, M. B. and Larson, H. J., "*Thick Thermal Barrier Coatings for Diesel Components*", *DOE/NASA/0332-1, NASA CR - 190759*, 1992.

[6] Zhu, D. and Miller, R. A., "*Evaluation of Oxidation Damage in Thermal Barrier Coating Systems*", *NASA Technical Memorandum 107360, Army Research Laboratory Technical Report ARL-TR-1254*, November 1996. Also in *Fundamental Aspects of High Temperature Corrosion* (eds. Shores, D. A.*et al*,), 289-307, **PV96-26**, The Electrochemical Society, Inc., Pennington, New Jersey, 1997.

[7] Zhu, D. and Miller, R. A., "*On Delamination Mechanisms of Thick Thermal Barrier Coating Systems under Thermal Fatigue Conditions", in preparation*, 1997.

[8] Takeuchi, Y. R. and Kokini, K., "*Thermal Fracture of Multilayer Ceramic Thermal Barrier Coatings", Journal of Engineering for Gas Turbines and Power*, **116**, 266-271, 1994.

[9] Kokini, K., Choules, D. B. and Takeuchi, Y., "*Thermal Fracture Mechanisms in Ceramic Thermal Barrier Coatings*" , in *Thermal Barrier Coating Workshop* (ed. Brindley, W. J.), 235-250, Cleveland, Ohio, March 27-29, 1995.

[10] Sidewell, C. V. and Cruse, T. A., "*Mechanical Testing Program for Thermal Barrier Coating Development*" , *Report 960801*, 1996.

[11] Zhu, D. and Miller, R. A., "*Influence of High Cycle Thermal Loads on Thermal Fatigue Behavior of Thick Thermal Barrier Coatings*", *NASA Technical Paper 3676, Army Research Laboratory Technical Report ARL-TR-1341*, March 1997.

[12] Kokini, K., Takeuchi, Y. R. and Choules, B. D., "*Surface Thermal Cracking of Thermal Barrier Coatings owing to Stress Relaxation: Zirconia vs. Mullite*", *Surface and Coatings Technology*, **82**, 77-82, 1996.

[13] Luxon, J. T. and Parker, D. E., "*Industrial Lasers and Their Applications*", Prentice-Hall, Inc., Englewood Cliffs, New Jersey, 1985.

[14] Johnsen, B. P., Cruse, T. A., Miller, R. A. and Brindley, W. J., "*Compressive Fatigue of a Plasma Sprayed ZrO_2-8%Y_2O_3 and ZrO_2-10%NiCrAlY TTBC*", *Journal of Engineering Materials and Technology*, **117**, 305-310, 1995.

[15] Wesling, K. F., Socie, D. F. and Beardsley, B., "*Fatigue of Thick Thermal Barrier Coatings*", *Journal of the American Ceramic Society*, **77**, 1863-1868, 1991.

[16] Thurn, G., Schneider, G. A. and Aldinger, F., "*High-temperature Deformation of Plasma-sprayed ZrO_2-Thermal Barrier Coatings*", *Materials Science and Engineering*, to be published, 1996.

[17] Murakami, Y., "*Stress Intensity Factors Handbook*", 108, Pergamon Press, Oxford, 1987.

REPORT DOCUMENTATION PAGE

Form Approved
OMB No. 0704-0188

1. AGENCY USE ONLY (*Leave blank*)	2. REPORT DATE	3. REPORT TYPE AND DATES COVERED
	June 1997	Technical Memorandum

4. TITLE AND SUBTITLE

Thermal Fatigue Testing of ZrO_2-Y_2O_3 Thermal Barrier Coating Systems Using a High Power CO_2 Laser

5. FUNDING NUMBERS

WU–523–21–13
1L161102AH45

6. AUTHOR(S)

Dongming Zhu and Robert A. Miller

7. PERFORMING ORGANIZATION NAME(S) AND ADDRESS(ES)

NASA Lewis Research Center
Cleveland, Ohio 44135–3191
and
U.S. Army Research Laboratory
Cleveland, Ohio 44135–3191

8. PERFORMING ORGANIZATION REPORT NUMBER

E–10704

9. SPONSORING/MONITORING AGENCY NAME(S) AND ADDRESS(ES)

National Aeronautics and Space Administration
Washington, DC 20546–0001
and
U.S. Army Research Laboratory
Adelphi, Maryland 20783–1145

10. SPONSORING/MONITORING AGENCY REPORT NUMBER

NASA TM–107439
ARL–TR–1354

11. SUPPLEMENTARY NOTES

Prepared for the International Conference on Metallurgical Coatings and Thin Films sponsored by the Vacuum Metallurgy Division and Thin Film Division of the American Vacuum Society, San Diego, California, April 21–25, 1997. Dongming Zhu, National Research Council—Research Associate at Lewis Research Center and Robert A. Miller, NASA Lewis Research Center. Responsible person, Dongming Zhu, organization code 5160, (216) 433–3161.

12a. DISTRIBUTION/AVAILABILITY STATEMENT

Unclassified - Unlimited
Subject Category 23

This publication is available from the NASA Center for AeroSpace Information, (301) 621–0390.

12b. DISTRIBUTION CODE

13. ABSTRACT ***(Maximum 200 words)***

In the present study, the mechanisms of fatigue crack initiation and propagation, and of coating failure, under thermal loads that simulate diesel engine conditions, are investigated. The surface cracks initiate early and grow continuously under thermal low cycle fatigue (LCF) and high cycle fatigue (HCF) stresses. It is found that, in the absence of interfacial oxidation, the failure associated with LCF is closely related to coating sintering and creep at high temperatures. Significant LCF and HCF interactions have been observed in the thermal fatigue tests. The fatigue crack growth rate in the ceramic coating strongly depends on the characteristic HCF cycle number, N^*_{HCF}, which is defined as the number of HCF cycles per LCF cycle. The crack growth rate is increased from 0.36 μm/LCF cycle for a pure LCF test to 2.8 μm/LCF cycle for a combined LCF and HCF test at N^*_{HCF} about 20,000. A surface wedging model has been proposed to account for the HCF crack growth in the coating systems. This mechanism predicts that HCF damage effect increases with increasing surface temperature swing, the thermal expansion coefficient and the elastic modulus of the ceramic coating, as well as with the HCF interacting depth. A good agreement has been found between the analysis and experimental evidence.

14. SUBJECT TERMS

Thermal barrier coatings; Thermal high cycle and low cycle fatigue; Ceramic sintering and creep; Characteristic HCF cycle number

15. NUMBER OF PAGES

30

16. PRICE CODE

A03

17. SECURITY CLASSIFICATION OF REPORT	18. SECURITY CLASSIFICATION OF THIS PAGE	19. SECURITY CLASSIFICATION OF ABSTRACT	20. LIMITATION OF ABSTRACT
Unclassified	Unclassified	Unclassified	